Photolytic Activity of Early Intermediates in Dioxygen Activation and Reduction by Cytochrome Oxidase

Constantinos A. Varotsis[†] and Gerald T. Babcock*[,‡]

Contribution from the Department of Chemistry, University of Crete, 71409, Iraklion, Crete, Greece, and The LASER Laboratory and Department of Chemistry, Michigan State University, East Lansing, Michigan 48824

Received October 7, 1994[⊗]

Abstract: Time-resolved resonance Raman spectra have been recorded during the reaction of fully reduced ($a^{2+}a_3^{2+}$) cytochrome oxidase with dioxygen at room temperature. We have monitored the $Fe^{2+}-O_2$ vibration at 571 cm^{-1} and the time course of reaction photolability. Our results indicate that, in addition to the $a_3^{2+}-O_2$ species, the following intermediate in the reaction sequence, which can be described as a peroxy species with a total of three reducing equivalents in the binuclear center, is also photolabile and can be photolyzed to regenerate the fully reduced enzyme. The apparent rate constant that we observe for the decay of photolytic activity is $\sim 10^4$ s^{-1}, which correlates with other relaxation phenomena that have been observed in the O_2 reduction reaction. We suggest that the underlying process that governs these phenomena is an input/output configurational transition associated with the proton-pumping activity of the enzyme. These results on the kinetics of the photolytic activity of the early intermediates in the cytochrome/O_2 reaction resolve apparent differences between our earlier results and interpretation of the oxidase/O_2 reaction time course and those of Blackmore, Greenwood, and Gibson (*J. Biol. Chem.* **1991**, *266*, 19245). We have also recorded Raman spectra in the low-frequency (200−500 cm^{-1}) region during the oxidase/O_2 reaction that show the $\nu(Fe^{2+}-his)$ stretching vibration in photoproducts that result from CO, O_2, and peroxy adduct photolysis. The photolysis products that can be generated during the O_2 reduction reaction have vibrational properties similar to those of the CO photolysis product, which suggests that the relaxation dynamics of heme a_3 following ligand photolysis are independent of ligand.

Introduction

Cytochrome oxidase sustains mitochondrial electron transport and linked ATP synthesis by catalyzing the four-electron reduction of dioxygen to water.[1] Substantial progress has been made recently in gaining a molecular level understanding of the structure of the enzyme and of the coordination of the two heme *A* irons and two copper ions that confer redox activity. Both of the hemes *A*, heme *a* and heme a_3, as well as one of the two copper ions, Cu_B, are bound to the heaviest subunit, subunit I. Recent directed mutagenesis work has identified the likely histidine ligands to these metal centers.[2] Heme a_3 and Cu_B comprise the binuclear center at which O_2 binding and reduction take place. Heme *a* links the binuclear center to the electron input stage of the protein, which, in the mammalian enzyme, is the second copper center, Cu_A,[3] bound to subunit II of the protein. A linear electron transport mechanism operates in the enzyme as follows:

$$\text{Cyt } c \rightarrow Cu_A \rightarrow a \rightarrow [a_3-O_2\ Cu_B]$$

where the final structure in the sequence indicates the oxygen-bound binuclear center at which the redox chemistry involved in reducing dioxygen to water takes place. Recent considerations have also implicated events in the binuclear center directly in the proton-pumping function of the enzyme.[4]

Among oxygen-metabolizing heme enzymes, cytochrome oxidase is unique in being susceptible to a high time resolution spectroscopic investigation of its reaction time course and of the intermediate, partially reduced oxygen structures that occur in the binuclear center during oxygen reduction. We interpreted this behavior to reflect a control mechanism, specific to cytochrome oxidase, that ensures efficient linkage of the spontaneous electron-transfer events associated with O_2 reduction to proton translocation against a concentration gradient.[5] In the most general scheme for O_2 reduction, both electron and proton transfer occur and intermediate species are expected:

$$O_2 \xrightarrow[e^-]{} \text{"intermediates"} \xrightarrow[H^+]{} 2H_2O$$

In most O_2-metabolizing enzymes, the electron transfer is rate limiting, protonation is fast, and potentially toxic intermediates do not accumulate to significant levels. In cytochrome oxidase, however, the proton transfers limit the reaction, the electron-transfer chemistry progressively slows down as the reaction proceeds, and tight coupling between the reduction process and proton translocation is assured. As a consequence, partially reduced dioxygen intermediates rise transiently to levels that are detectable by spectroscopic techniques.

Both time-resolved optical[6] and resonance Raman spectroscopies[7] have been used to exploit this situation in Gibson−Greenwood type flow/flash experiments at room temperature. Low-temperature trapping and subsequent ERPR spectroscopic

[†] University of Crete.
[‡] Michigan State University.
[⊗] Abstract published in *Advance ACS Abstracts*, October 15, 1995.

(1) Wikström, M.; Krab, K.; Saraste, M. *Cytochrome Oxidase-A Synthesis*; Academic Press: New York, 1981.
(2) Hosler, J. P.; Ferguson-Miller, S.; Calhoun, M. W.; Thomas, J. W.; Hill, J.; Lemieux, L.; Ma, J.; Georgiou, C.; Fetter, J.; Shapleigh, J.; Tecklenburg, M. M. J.; Babcock, G. T.; Gennis, R. B. *J. Bioenerg. Biomembr.* **1993**, *25*, 121−136.
(3) Hill, B. C. *J. Biol. Chem.* **1991**, *266*, 2219−2226.
(4) (a) Babcock, G. T.; Wikström, M. *Nature* **1992**, *356*, 301−309. (b) Wikström, M.; Babcock, G. T. *Nature* **1990**, *348*, 16−17.
(5) (a) Babcock, G. T.; Varotsis, C.; Zhang, Y. *Biochim. Biophys. Acta* **1992**, *1101*, 192−194. (b) Babcock, G. T.; Varotsis, C. *Biomol. Spectrosc.* **1993**, *1890*. (c) Babcock, G. T.; Varotsis, C. *J. Bioenerg. Biomembr.* **1993**, *25*, 2, 71−80. (d) Babcock, G. T. *Encyclopedia of Inorganic Chemistry*; Scott, R. H., Ed.; Wiley: New York, in press.

0002-7863/95/1517-11260$09.00/0

examination have also been applied to the O_2/enzyme reaction.[8] In an alternative approach, Wikström has been able to reverse the forward reaction to generate fairly stable forms of several transient species.[9] From this work, molecular structures have been proposed for several of the intermediates in the reaction. These include heme a_3 iron-bound oxy, peroxy, ferryl, and hydroxyl species that occur at various stages in the mechanism.[4] There appears now to be general consensus as to the occurrence of these species, although the precise details of their molecular structures remain to be determined unambiguously. The reaction sequence for the O_2/cytochrome oxidase reaction that we deduced from these developments is summarized in the scheme in Figure 1, where the numbering of various intermediates in the cycle is preserved from ref 4. Rate constants have been assigned to key steps, and we have used these to model the full reaction time course.[7e]

Within this mechanism, two distinct operations can be discerned. The initial fast phase involves O_2 binding and partial reduction to capture the substrate in the binuclear center as a peroxy species (**3** in Figure 1). Following this rapid trapping process and the conformational relaxation associated with the pump function, the third and fourth electrons are transferred to peroxy (**3′**) and ferryl (**7**) intermediates, respectively, in exergonic redox reactions that drive the proton pump in the second phase of the dioxygen reduction process. The proton pumping steps are indicated by the darker arrows in Figure 1. In flow/flash experiments with the fully reduced enzyme, there appears to be a short-circuiting reaction that is initiated by the reduction of **3** by heme *a* to form **4** in times short compared to that

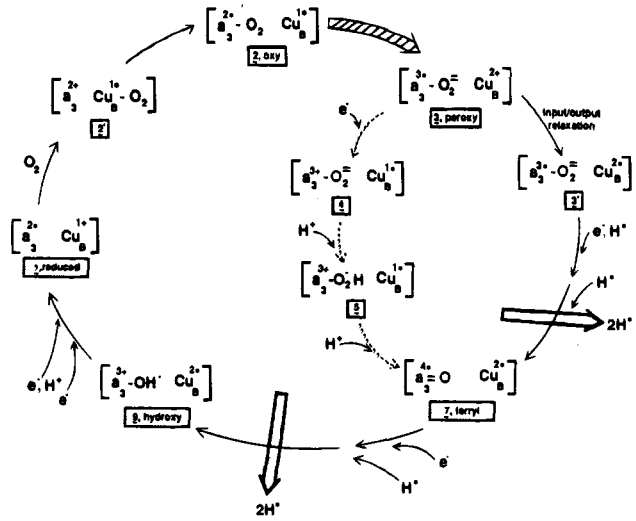

Figure 1. Reaction sequence for the cytochrome oxidase/O_2 reaction. Only the iron and copper ions of the binuclear center are shown.

required for the **3** → **3′** conformational relaxation. This pathway is uncoupled from proton pumping and is shown by the dashed arrows in Figure 1. Under these conditions, the rate constants for the formation and decay of the two-electron reduced peroxy species **3** are such that it does not accumulate to substantial levels. The short-circuited route rejoins the coupled pathway as the three-electron-reduced peroxy intermediate **4** is protonated to initiate the oxygen−oxygen bond cleavage process that produces the ferryl intermediate **7**. Recent data from Wikström and co-workers[6l] have indicated that an equilibrium may be established that involves **1**−**3**, when the fully reduced enzyme reacts with O_2, i.e., that, in this situation, O_2 is trapped irreversibly only when **4** is formed.

Although the scheme in Figure 1 generally describes the reaction sequence, there is ambiguity as to details of the dioxygen-trapping reactions. Our initial work showed that the oxy species **2** is formed in the first 10 μs of the reaction and is photolabile;[7a,b] its $\nu(Fe^{2+}-O_2)$ vibration is detected at 572 cm^{-1}.[7b,f,h] Subsequent time-resolved Raman data showed that the short-circuiting electron transfer from heme *a* to form **4** occurs with a rate constant of 3×10^4 s^{-1}.[7d,f] These observations predict that the oxy complex forms quickly and reaches maximal concentration at 25−30 μs in the reaction.[7e] Blackmore *et al.*, however, monitored photolability optically and found that photosensitivity maximizes at 60−70 μs following CO photolysis.[6h] To accommodate these results, as well as their observations that O_2 binding shows saturation kinetics, they postulated transient formation of a Cu_B-O_2 intermediate (**2′** in Figure 1) that precedes O_2 binding at a_3 (see, also, refs 10−13). Subsequent transfer of the oxy ligand to a_3 to form **2** was postulated to occur at substantially slower rates than indicated by the Raman data discussed above. Oliveberg and Malmström[6g] have also interpreted recent time-resolved optical data to indicate a relatively long-lived Cu_B-O_2 intermediate. These models, while in qualitative agreement with the Raman data, predict significantly longer lifetimes for **2′** and **2** than can be accommodated in a quantitative interpretation of the vibrational results.

To provide better resolution of the initial O_2 binding and trapping chemistry, we have used flow/flash, time-resolved resonance Raman techniques to investigate early events in the cytochrome oxidase/O_2 reaction. In the work described here, we monitored both the $Fe^{2+}-O_2$ vibration and the time course of reaction photolability. In addition, we have detected the $\nu(Fe^{2+}-his)$ in photoproducts that result from carbon monoxide and dioxygen adduct photolysis. Our results confirm rapid

(6) (a) Gibson, Q. H.; Greenwood, C. *Biochem. J.* **1963**, *86*, 541−554. (b) Greenwood, G.; Gibson, Q. H. *J. Biol. Chem.* **1967**, *242*, 1782−1787. (c) Hill, B. C.; Greenwood, C. *Biochem. J.* **1984**, *218*, 913−921. (d) Hill, B. C.; Greenwood, C.; Nicholls, P. *Biochem. Biophys. Acta* **1986**, *853*, 91−113. (e) Orii, Y. *Ann. N.Y. Acad. Sci.* **1988**, *550*, 105−117. (f) Oliveberg, M.; Brzezinski, P.; Malmström, B. G. *Biochim. Biophys. Acta* **1989**, *977*, 322−328. (g) Oliveberg, M.; Malmström, B. G. *Biochemistry* **1992**, *31*, 3560−3563. (h) Blackmore, R. S.; Greenwood, C.; Gibson, Q. H. *J. Biol. Chem.* **1991**, *266*, 19245−19249. (i) Oliveberg, M.; Hallén, S.; Nilsson, T. *Biochemistry* **1991**, *30*, 436−440. (j) Hallén, S.; Nilsson, T. *Biochemistry* **1992**, *31*, 11853−11859. (k) Svensson, M.; Nilsson, T. *Biochemistry* **1993**, *32*, 5442−5447. (l) Verkhovsky, M. I.; Morgan, J. E.; Wikström, M. *Biochemistry* **1994**, *33*, 3079−3086.

(7) (a) Babcock, G. T.; Jean, J. M.; Johnston, L. N.; Palmer, G.; Woodruff, W. H. *J. Am. Chem. Soc.* **1984**, *106*, 8305−8306. (b) Varotsis, C.; Woodruff, W. H.; Babcock, G. T. *J. Am. Chem. Soc.* **1989**, *111*, 6439−6440; **1990**, *112*, 1297. (c) Varotsis, C.; Woodruff, W. H.; Babcock, G. T. *J. Biol. Chem.* **1990**, *265*, 11131−11136. (d) Varotsis, C.; Babcock, G. T. *Biochemistry* **1990**, *29*, 7357−7362. (e) Varotsis, C.; Zhang, Y.; Appelman, E. H.; Babcock, G. T. *Proc. Natl. Acad. Sci. U.S.A.* **1993**, *90*, 237−241. (f) Han, S.; Ching, Y.-C.; Rousseau, D. L. *Proc. Natl. Acad. Sci. U.S.A.* **1990**, *87*, 2491−2495. (g) Han, S.; Ching, Y.-C.; Rousseau, D. L. *Nature* **1990**, *348*, 89−90. (h) Ogura, T.; Takahashi, S.; Shinzawa-Itoh, K.; Yoshikawa, S.; Kitagawa, T. *J. Am. Chem. Soc.* **1990**, *112*, 5630−5631. (i) Ogura, T.; Takahashi, S.; Shinzawa-Itoh, K.; Yoshikawa, S.; Kitagawa, T. *Bull. Chem. Soc. Jpn.* **1991**, *64*, 2901−2907. (j) Ogura, T.; Takahashi, S.; Hirota, S.; Shinzawa-Itoh, K.; Yoshikawa, S.; Appelman, E. H.; Kitagawa, T. *J. Am. Chem. Soc.* **1993**, *115*, 8527−8536. (k) Proshlyakov, D. A.; Ogura, T.; Shinzawa-Itoh, K.; Yoshikawa, S.; Appelman, E. H.; Kitagawa, T. *J. Biol. Chem.* **1994**, *269*, 29385−29388.

(8) (a) Chance, B.; Saronio, C.; Leigh, J. S., Jr. *J. Biol. Chem.* **1975**, *250*, 9226−9237. (b) Clore, G. M.; Andreasson, L. E.; Karlsson, B.; Aasa, R.; Malmström, B. G. *Biochem. J.* **1980**, *185*, 139−154. (c) Blair, D. F.; Witt, S. N.; Chan, S. I. *J. Am. Chem. Soc.* **1985**, *107*, 7389−7399.

(9) (a) Wikström, M. *Proc. Natl. Acad. Sci. U.S.A.* **1981**, *78*, 4051−4054. (b) Wikström, M. *Chem. Scr.* **1987**, *278*, 53−58. (c) Wikström, M. *Chem. Scr.* **1988**, *28A*, 71−71. (d) Wikström, M. *FEBS Lett.* **1988**, *231*, 247−252. (e) Wikström, M. *Nature* **1989**, *338*, 776−778.

(10) Woodruff, W. H.; Dyer, R. B.; Einarsdottir, O. In *Biological Spectroscopy*; Clark, R. J. H., Hester, R. E., Eds.; John Wiley and Sons, Ltd.: Chichester, England, 1993; Part B, pp 189−223.

(11) Woodruff, W. H.; Einarsdottir, O.; Dyer, R. B.; Bagley, K. A.; Palmer, G.; Atherton, S. J.; Goldbeck, R. A.; Dawes, T. D.; Kliger, D. S. *Proc. Natl. Acad. Sci. U.S.A.* **1991**, *88*, 2588−2592.

(12) Woodruff, W. H. *J. Bioenerg. Biomembr.* **1993**, *25*, 177−188.

(13) Dyer, R. B.; Peterson, K. A.; Stoutland, P. O.; Woodruff, W. H. *Biochemistry* **1994**, *33*, 500−507.

formation of the heme a_3-O_2 adduct. Moreover, we make the surprising observation that, in addition to the oxy species **2**, the three-electron-reduced peroxy species **4** is also photolabile and can be photolyzed to regenerate the fully reduced enzyme. Our observations that both the oxy and peroxy species are photolabile reconciles apparent differences between our work and that of Blackmore *et al.*[6h] The photolysis products that can be formed during dioxygen reduction have transient vibrational properties analogous to those of the CO photolysis product, which suggests that relaxation dynamics in the binuclear center following ligand photodissociation are independent of ligand.

Experimental Procedures

Cytochrome oxidase was prepared from beef hearts by using a modified Hartzell–Beinert procedure[7a] and was frozen under liquid N_2 until ready for use. The enzyme was solubilized in 50 mM HEPES [4-(2-hydroxyethyl)-1-piperazineethanesulfonic acid] at pH 7.4 with 0.5% dedecyl β-D-maltoside. The fully reduced, carbon monoxide bound enzyme was prepared by anaerobic reduction, with 4 mM sodium ascorbate and 1 μM cytochrome *c* under CO, and showed a Soret maximum at 430 nm, as expected.

The experimental techniques used for the measurements of time-resolved Raman spectra during the oxidation of reduced cytochrome oxidase by dioxygen at room temperature have been reported.[7e,14] The probe wavelengths, 416 and 435.7 nm, were produced by Stokes Raman shifting the third harmonic and by anti-Stokes Raman shifting the second harmonic of a Quanta Ray DCR-2A Nd:YAG laser in H_2, respectively. The probe wavelength, 427 nm, was provided by pumping stilbene 420 with the third harmonic output (355 nm). The enzyme concentration, after mixing, was 80 μM when 416-nm excitation was used; with 427- and 435.7-nm excitations, the concentration was decreased to 50 μM. For the low-energy Raman measurements, approximately ten photons per pulse oxidase molecule in the scattering volume were incident; this was increased by a factor of 10 for the high-energy measurements.

Results

Figure 2B–D shows time-resolved resonance Raman spectra in the high-frequency region recorded at 10, 50, and 100 μs, respectively, after initiating the reaction between fully reduced cytochrome oxidase and dioxygen. Figure 2A shows the spectrum of the reduced enzyme. All spectra were obtained with a low-energy, defocused beam to minimize photolysis of the heme a_3/O_2 species. In the reduced spectrum (Figure 2A), the oxidation state marker, ν_4, is located at 1355 cm^{-1}, characteristic of hemes *a* and a_3 in their ferrous states. The core size sensitivity ν_2 bands are located at 1570 cm^{-1} (heme a_3) and 1586 cm^{-1} (heme *a*). The 1613- and 1666-cm^{-1} modes have been assigned as the C=O stretching vibration of the formyl groups of hemes a^{2+} and a_3^{2+}, respectively. The 10-μs spectrum shows that extensive changes have occurred in the vibrational properties of *a* and a_3 at this early time in the reaction with dioxygen. The oxidation state marker band has shifted to 1371 cm^{-1}, the 1570-cm^{-1} ν_2 mode has lost intensity at the expense of the 1589-cm^{-1} vibration, and the a_3^{2+} formyl ν(C=O) stretch in the reduced enzyme has shifted to 1670 cm^{-1}. These changes indicate the formation of oxy heme a_3 (**2**) at 10 μs, as shown earlier[7b] (see also below). In addition to the a_3 oxygen addition reaction, oxidation of heme *a* is also apparent in the 10-μs spectrum. This is most clearly seen in the shift of the heme *a* formyl stretching vibration from 1613 cm^{-1} in the reduced enzyme to 1650 cm^{-1}, which is its frequency in oxidized heme *a* (see Figure 3F). The 1640-cm^{-1} ν_{10} vibration in the 10-μs spectrum also arises from the oxidized low-spin heme *a* center. The 1355-cm^{-1} shoulder on the 1371-cm^{-1} peak, however, shows that these processes are not complete at

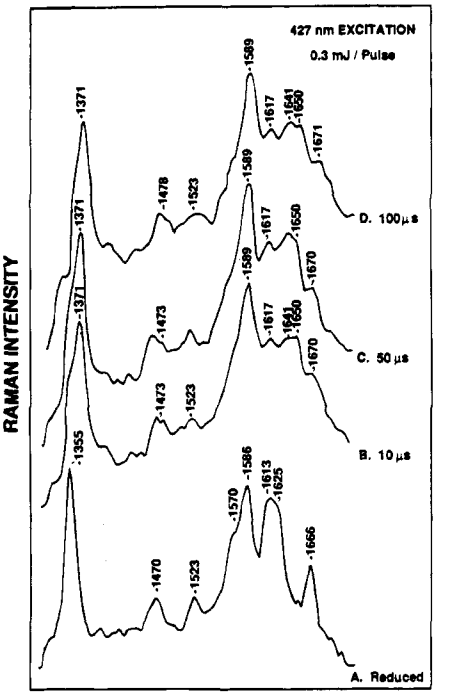

Figure 2. Time-resolved resonance Raman spectra of fully reduced cytochrome oxidase at the indicated times. The energy of the 532-nm photolysis pump/pulse was 1.3 mJ, sufficient to photolyze the oxidase–CO complex and initiate the O_2-reduction reaction. The energy of the 427-nm-probe beam was 0.3 mJ/pulse. The repetition rate for both the pump and probe pulses was 10 Hz. The accumulation time was 15 min for spectrum A and 50 min for spectra B–D.

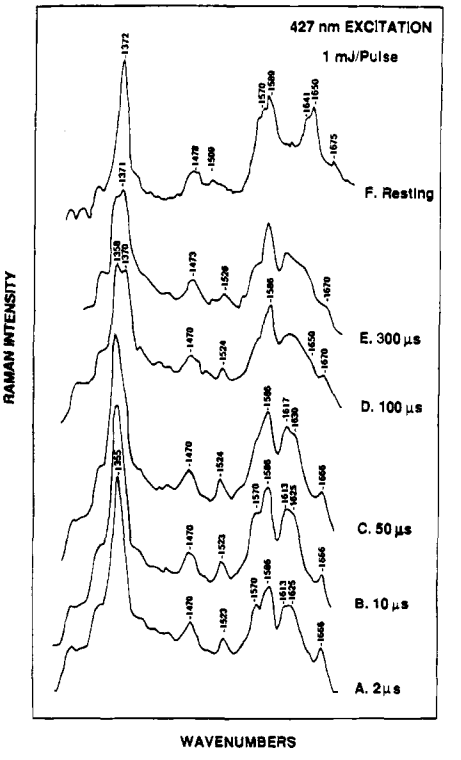

Figure 3. Time-resolved resonance Raman spectra of fully reduced cytochrome oxidase at the indicated times. The energy of the 532-nm photolysis pump/pulse was 1.3 mJ. The energy of the 427-nm-probe beam was 1 mJ/pulse. The repetition rate for both the pump and probe pulses was 10 Hz. The accumulation time was 15 min for all spectra.

(14) (a) Varotsis, C.; Oertling, W. A.; Babcock, G. T. *Appl. Spectrosc.* **1990**, *44*, 742–744. (b) Varotsis, C.; Babcock, G. T. *Methods Enzymol.* **1993**, *226C*, 409–431.

10 μs. This feature becomes less pronounced in the 50- and 100-μs spectra, indicating that heme *a* oxidation continues on this time scale. These observations are consistent with earlier work,[7d,f] from which the short-circuited formation of the three-electron-reduced peroxy species (**4** in Figure 1) has been deduced.

In Figure 3 (traces A–E), we present a similar set of spectra of fully reduced cytochrome oxidase at various delay times (2–300 μs) after initiation of dioxygen reduction. Also shown is the spectrum of the oxidized, resting enzyme (trace F). These data, however, were obtained with higher intensity probe pulses that were more tightly focused on the sample scattering volume. As the reaction proceeds, oxidation of hemes *a* and a_3 is expected to take place according to the same time course that occurred in Figure 2. In Figure 3, however, there is little change in the position of the oxidation state marker, ν_4, and the formyl vibrations, even at 50 μs following initiation of the reaction. These results are consistent with our earlier work showing that photolabile intermediates are generated in the initial stages of dioxygen reduction and that these intermediates can be photolyzed by the Raman probe pulse, if its energy is sufficiently high, to produce the unliganded, reduced enzyme according to Scheme 1,

Scheme 1

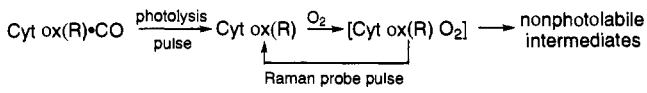

where Cyt ox(R) represents the reduced protein and [Cyt ox(R) O_2] the initial, photolabile species. Only at 100 and 300 μs (Figure 3, traces D and E, respectively) does ν_4 indicate a substantial shift to 1371 cm^{-1}. In these latter spectra, the intensity of the 1358-cm^{-1} mode has substantially decreased, indicating generation of nonphotolabile forms of the enzyme. The core size sensitive band (ν_2) of heme a_3 shifts to higher frequency and overlaps with the ν_2 low-spin vibration of heme *a* at 1588 cm^{-1}; the formyl modes of both *a* and a_3 lose intensity at frequencies characteristic of their reduced forms and exhibit increased scattering at frequencies (1650 and ~1670 cm^{-1}) that are characteristic of the oxidized chromophores. Comparison of the 100-μs spectra in Figures 2 and 3 indicates, however, that the ratio of 1371 cm^{-1}/1355 cm^{-1} intensities is significantly higher in the low-pulse-energy measurements (Figure 2), which shows that a relatively high population of photolabile species remains at this time.

The data in Figures 2 and 3 shed new light on the identity of photolabile intermediates in the reduction of O_2 by cytochrome oxidase. In the interpretation of our earlier Raman data,[7a,b] as well as in the optical experiments reported by Blackmore *et al.*,[6h] oxy heme a_3 was implicitly assumed to be the only photolabile intermediate in the reaction. This assumption is consistent with the fairly rapid decay of photolability observed in these experiments, but the occurrence of rapid heme *a* oxidation to form **4** according to the short-circuiting pathway shown in Figure 1 was not understood at the time. The 10-μs spectrum in Figure 2 confirms the fast heme *a* oxidation reaction and the corresponding 10-μs spectrum in Figure 3 shows that

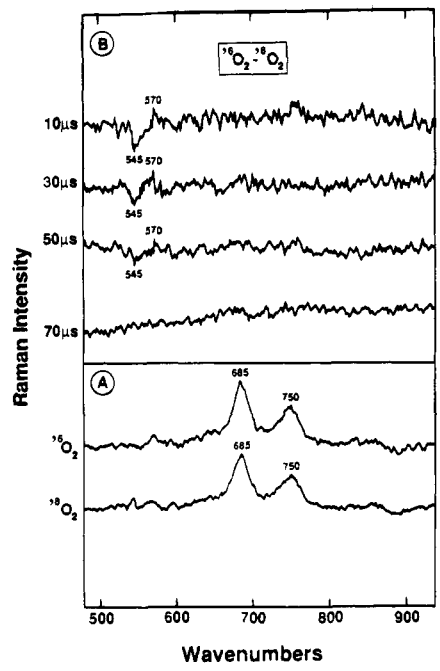

Figure 4. (A) Time-resolved resonance Raman spectra of fully reduced cytochrome oxidase following initiation of reaction with oxygen at room temperature. The energy of the 532-nm photolysis pump pulse was 1.3 mJ. The energy of the probe beam was 0.3 mJ. The repetition rate of both the pump and probe pulses was 10 Hz. The pump-probe delay was 10 μs. (B) Difference spectra (transient spectrum recorded with $^{16}O_2$ as the substrate minus transient spectrum with $^{18}O_2$ as the substrate) of initial intermediates in the reaction of fully reduced cytochrome oxidase observed at the indicated times.

this fast oxidation can be photoreversed. These data demonstrate that photolability in the O_2 reduction reaction extends beyond the oxy adduct to intermediates in which heme *a* has injected a third electron into the binuclear center. We conclude that both the oxy species **2** and the three-electron-reduced species **4** in Figure 1 are photolabile; photolysis of **4** photoreverses the rapid oxidation of heme *a* according to Scheme 2.

Within the context of Scheme 2, simulations of the reaction time course predict that the oxy species will decay more rapidly than reaction photolability, as we have assigned decay rate constants of 3×10^4 s^{-1} for **2** and 1×10^4 s^{-1} for **4**.[4,7e] Han *et al.* have presented Raman data on the lifetime of **2** that are consistent with this suggestion.[7f] In Figure 4, we monitor the time course of the $\nu(Fe-O_2)$ vibration directly as a means by which to assess the formation and decay of **2**. The two traces in panel A of Figure 4 are absolute spectra in the low-frequency region at 10 μs in the reduced cytochrome oxidase–O_2 reaction when $^{18}O_2$ and $^{16}O_2$ are used to oxidize the enzyme. By subtracting the $^{18}O_2$ spectrum from the $^{16}O_2$ spectrum, the 10-μs difference spectrum is obtained as shown in panel B of Figure 4. The 571-cm^{-1} peak/546-cm^{-1} trough in the difference spectrum is the $\nu(Fe-O_2)$ vibration of oxycytochrome a_3. The three other traces in panel B show the corresponding difference spectra at 30, 50, and 70 μs in the reaction sequence. In agreement with earlier data and with the high-frequency spectra in Figure 2, the 10- and 30-μs spectra show significant oxy heme

Scheme 2

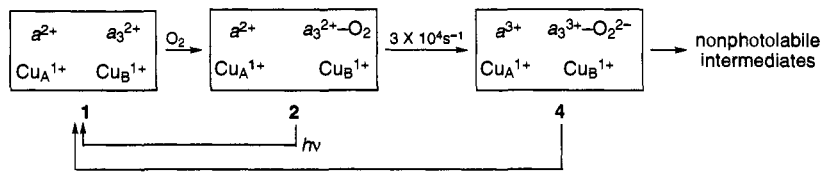

a_3 concentrations.[7a,b,e,f] By 50 μs this species has decayed substantially, as expected for the 3×10^4 s^{-1} rate constant deduced for heme *a* oxidation, to form **4**, and at 70 μs at the oxy intermediate is no longer detectable with our signal/noise capability. These results, in comparison with those in Figure 3, are consistent with the model in Scheme 2, as the decay of **2** precedes the disappearance of photolability in the dioxygen reduction reaction.

In earlier work on the photodissociation of CO from fully reduced cytochrome oxidase, Findsen *et al.*[15] showed that the Fe–histidine vibration of ferrous deoxy heme a_3 could be detected following CO photolysis. In these experiments, the ν(Fe–his) vibration was observed at 221 cm^{-1} in the photolysis product; this mode shifted to its 215-cm^{-1} equilibrium value as the relaxation proceeded, which was interpreted according to Scheme 3

Scheme 3

$$a_3\text{–CO} \xrightarrow{h\nu} (a_3)^{**} \xrightarrow{\text{relaxation}} a_3$$

where $(a_3)^{**}$ denotes the non-equilibrium photolysis product and a_3 represents the relaxed equilibrium chromophore. Subsequent work by Woodruff *et al.*[11] confirmed the detection of the perturbed Fe–his mode in the CO photolysis product, although they noted that its intensity was a function of the Raman probe energy (see below). The data in Figures 2 and 3 indicate that photolysis of intermediates **2** and **4** in Figure 1 regenerates the fully reduced, deoxy enzyme. If this is the case, then we should be able to detect the Fe–histidine stretching vibration that is characteristic of five-coordinate, high-spin ferrous heme a_3 in the photolysis product in direct analogy to the earlier CO photolysis work. Figure 5 shows the low-frequency Raman spectrum of the equilibrium reduced oxidase and time-resolved spectra at various delay times subsequent to ligand photolysis from the CO-bound reduced derivative in the absence and presence of O_2. In the deoxy enzyme (Figure 5A), the Fe–his stretching vibration is observed at 215 cm^{-1}, characteristic of the relaxed form of reduced cytochrome oxidase. Upon CO photolysis, this mode is observed at 221 cm^{-1} at 10 ns after photodissociation (Figure 5B), in agreement with the Findsen *et al.* data.[15] Photolysis of **2** and **4** (Figure 5C–G) shows that similar behavior is observed for their photolysis products. At 20 and 40 μs following initiation of the dioxygen reduction reaction, photodissociation produces essentially complete regeneration of the Fe–his vibration (spectra C and D). Moreover, this mode is observed at 221 cm^{-1}, indicating that the photolysis product is initially generated in an unrelaxed configuration. These observations indicate that Scheme 3 above can be elaborated in analogy with the CO photolysis process to include the unrelaxed a_3 photoproduct, as follows:

$$\mathbf{2, 4} \xrightarrow{h\nu} (a_3)^{**} \xrightarrow{\text{relaxation}} a_3$$

where **2** and **4** refer to the oxy and three-electron reduced intermediates in Figure 1 and Scheme 2 and $(a_3)^{**}$ represents the unrelaxed deoxy form of a_3.

In these experiments, as in those in Figure 3, the second laser pulse both photodissociates the bound ligand and produces Raman scattering from the photolysis product. Thus, the time over which $(a_3)^{**}$ is interrogated in Figure 5 is determined by the laser pulse duration, here 10 ns. Spectra E, F, and G in

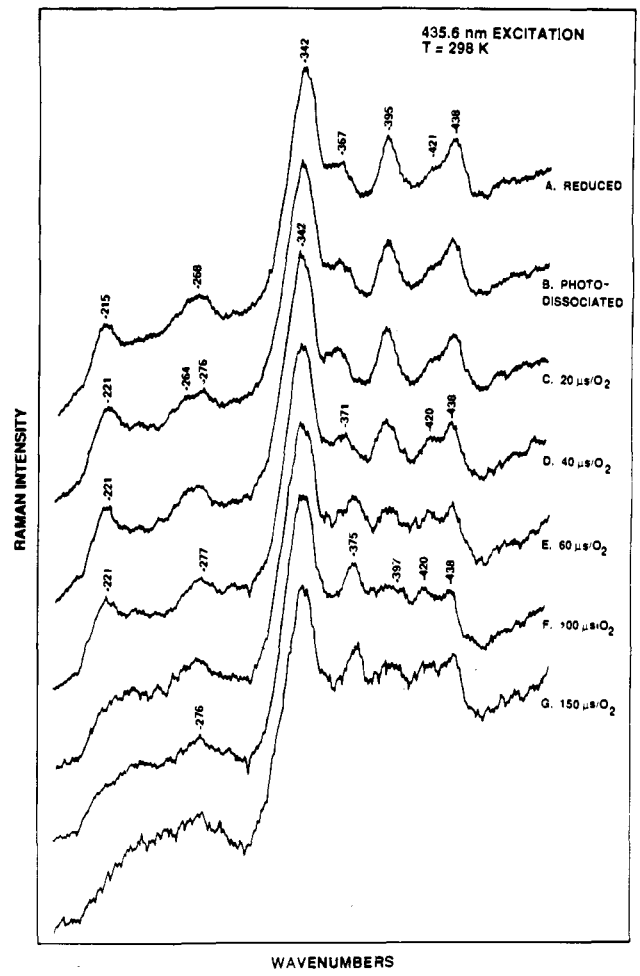

Figure 5. Low-frequency resonance Raman spectra of equilibrium-reduced oxidase (trace A) and time-resolved spectra at various delay times subsequent to ligand photolysis from the CO-bound reduced derivative in the absence (trace B) and presence of O_2 (traces C–G). All other conditions were the same as for Figure 3.

Figure 5 show that the extent to which the Fe–his vibration can be regenerated decreases as the delay between the pump pulse that initiates the dioxygen reduction reaction and the photodissociation/probe pulse increases. At 60 μs, full regeneration is no longer observed and this diminishes further at 100 and 150 μs. The low-frequency data in Figure 5 and the high-frequency data in Figure 3 are consistent in showing that photodissociable intermediates in the cytochrome oxidase–O_2 reaction are replaced by photostable species on the 100 μs time scale.

Figure 6 compares the decay of photolability, as measured by the intensity of the 221-cm^{-1} mode in Figure 5, with the decay of the oxy species from the difference spectra in Figure 4. The experimental data points for the concentration of the oxy species are compared to the calculated time course for the formation and decay of **2** from the model we presented earlier[4,7e] (solid line); experiment and calculation were normalized at the 30-μs point. The predicted kinetic behavior of the oxy species **2** fits the experimental data well; the most apparent discrepancy occurs at 70 μs and is likely to reflect both the relatively poor signal to noise in the data and partial photolysis of the oxy species, even by the low-intensity probe pulse.

The experimental data in Figure 6 for the decay of photolability show that photosensitivity, as measured by the light-induced regeneration of the Fe–his mode characteristic of the five-coordinate deoxy heme a_3 species, persists for substantially longer times than the oxy species, consistent with the high-

(15) Findsen, E. W.; Centeno, J.; Babcock, G. T.; Ondrias, M. R. *J. Am. Chem. Soc.* **1987**, *109*, 5367–5372.

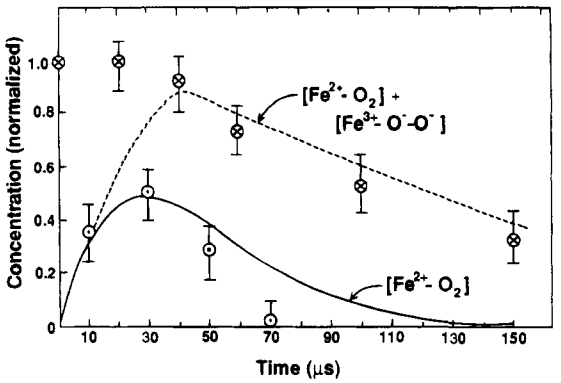

Figure 6. Comparison of the photolability decay (⊗) to the decay of the oxy species (○). The solid line indicates the time courses predicted from ref 7e for the time−concentration behavior of the oxy (**2**) species. The dashed line shows the time course calculated in ref 7e for the time−concentration behavior of the sum of oxy (**2**) and peroxy (**4**) species.

frequency data in Figure 3. In keeping with the hypothesis advanced above that both the oxy (**2**) and the three-electron reduced peroxy species (**4**) are photodissociable, we compare the experimental photodissociation data with the concentration−time profile for the sum of species **2** and **4** predicted from our kinetic model for the reaction−time course.[7e] The calculated curve is shown as the dashed line in Figure 6. The calculated curve peaks near 45 μs, and its decay follows that of the photolability decline fairly well. The experimental points are 5−10% lower than predicted, which probably indicates that we do not achieve complete photodissociation with the Raman probe pulses. At early times, full intensity of the Fe−his mode is observed because both **1** and **2**, as well the photodissociation products, are present.

Discussion

With the application of flow/flash time-resolved optical and Raman techniques by several labs, the mechanism of dioxygen activation by cytochrome oxidase is coming into sharper focus. There are, however, discrepancies and ambiguities in interpretation, as discussed above. The data presented here provide good resolution of the initial O_2-binding and electron-transfer steps in the process and support the kinetic scheme proposed for the reaction, as summarized in Figure 1. They also demonstrate surprising photoactivity for the early dioxygen intermediates that help resolve interpretational differences. In the sections below, we discuss first the reaction kinetics and then consider the photolability in more detail.

Formation of the Oxy Species 2. The Raman data in Figures 2 and 4 confirm earlier work that showed substantial formation of the $a_3^{2+}-O_2$ species at 10 μs, consistent with a first-order rate constant that approaches 10^5 s^{-1}. This rate corresponds well with the kinetics of the F_1 optical phase reported by Oliveberg *et al.*,[6f] which has a maximal rate of 9×10^4 s^{-1}. Moreover, the magnitude of this phase, which accounts for approximately 40% of the total Soret change during the reoxidation reaction, is consistent with O_2 association with a_3, but not with Cu_B, and accordingly can be assigned to the binding of O_2 to heme a_3. Blackmore *et al.*,[6h] Oliveberg and Malmström,[6g] and Verkhovsky *et al.*[6l] have shown that the O_2/a_3 reaction exhibits saturable kinetics. In accord with suggestions from Woodruff *et al.*,[11] all three groups interpreted this behavior to reflect diffusional association of O_2 with Cu_B followed by a first-order transfer to the a_3 site; Blackmore *et al.*[6h] assigned a rate constant of 3.5×10^8 M^{-1} s^{-1} for the Cu_B/O_2 association. Taken together, these results indicate that the dioxygen association process can be summarized as in Scheme 4. This mode fits well with the Raman data reported above and elsewhere. Moreover, it provides a mechanistic basis for the long-standing supposition made in analogy with CO-binding behavior, that both Cu_B and a_3 must be in their reduced states prior to dioxygen binding.[4a] Recent NO-binding data[6h] show that the a_3 site is uncluttered and capable of exogenous ligand binding at pseudo-first-order rates of at least 10^5 s^{-1}, which is also consistent with Scheme 4. Moreover, both the NO and O_2 binding data indicate that, if the ligand switching model proposed by Woodruff and co-workers[11,12] is correct, the rate of endogenous ligand dissociation must occur in less than a few microseconds for these exogenous ligands.

Decay of the Oxy Species. The decay of **2**, shown in Figure 4 and 6, is fit well by the 3×10^4 s^{-1} rate constants assigned earlier to this reaction on the basis of Raman data.[7d,f] The vibrational results showed both heme *a* oxidation and oxy heme a_3 decay with this rate constant, which led to the conclusion that electron transfer from *a* to the binuclear center occurred during this phase. This interpretation rationalized the F_2 optical change monitored by Oliveberg *et al.*,[6f] which occurred at an apparent rate constant of 3×10^4 s^{-1} and accounted for an additional 50% of the Soret bleaching at 445 nm, as the magnitude of the absorption change is indicative of heme *a* oxidation. Verkhovsky *et al.* recently reexamined this phase and similarly concluded that it represents injection of the third electron into the binuclear center; their analysis shows that this step corresponds to the first strongly driven reaction in the O_2-binding process.[6l]

Babcock and Wikström have argued recently that the 3×10^4 s^{-1} rate of heme *a* oxidation by the binuclear center reflects a slip in the proton translocating mechanism of the oxidase.[4] They suggested that this electron transfer occurs with a rate that is faster than the output/input conformational relaxation required for coupling and, thus, that it effectively short circuits participation of the two electron-reduced peroxy species (**3** in Figure 1) in the proton-pumping cycle. The origin of the slip was attributed to using the fully reduced enzyme, which is an unphysiological state of the protein, to reduce O_2. In this starting state, electron transfer from Cu_B to the oxy complex, to form **3**, was proposed to trigger rapid *a* oxidation so that the peroxy complex did not accumulate to detectable levels. Recent work by Verkhovsky *et al.*[16] supports this idea, as they showed that electron transfer between heme *a* and heme a_3, in their electronic ground states, occurred at a rate of at least 2.4×10^5 s^{-1}, which is almost an order of magnitude greater than the apparent 3×10^4 s^{-1} rate constant we observe for the coupled heme *a* oxidation and oxy decay. Taken together, these results suggest that Cu_B oxidation, which produces **3**, occurs at the 3×10^4 s^{-1} rate and is followed by heme *a* oxidation at rates greater than or equal to 2.4×10^5 s^{-1}. These steps are summarized in Scheme 5. With these rate constants, **4** would appear with the 3×10^4 s^{-1} rate constant and **3** would not be detected in a time-resolved experiment (see, also, ref 6l).

In Scheme 5, we have drawn both peroxy species **3** and **4** as deprotonated. Time-resolved optical work by Hallén and Nilsson,[6j] however, showed that the 3×10^4 s^{-1} phase, although not accompanied by proton uptake from solution, exhibits a relatively large deuterium isotope effect. They interpreted this to reflect proton transfer to the peroxy species from an acid/base group in the binuclear center that was protonated prior to initiating the reaction. The occurrence of a protonated site in the fully reduced enzyme is consistent with recent work by

(16) Verkhovsky, M. I.; Morgan, J. E.; Wikström, M. *Biochemistry* **1992**, *31*, 11860−11863.

Scheme 4

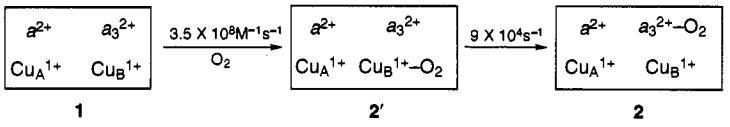

Scheme 5

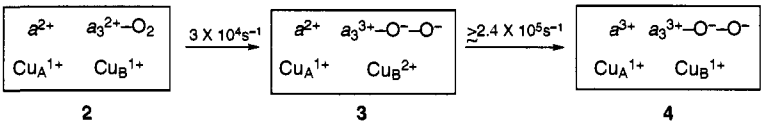

Mitchell and Rich[17] and has been invoked by Morgan *et al.*[18] in constructing a histidine-based protom pump in the enzyme. At present, we cannot assess whether transfer of this bound proton to the peroxy species occurs, as neither **3** nor **4** has been detected directly by Raman spectroscopy, which has the potential to assign ligand protonation state. We note, however, that that protonation reaction postulated by Hallén and Nilsson would facilitate the oxidation of heme *a* by **3** and may provide a basis for the fast **3** → **4** transition in Scheme 5.

Reaction Photolability and Its Decay. Blackmore *et al.*[6h] confirmed the photolability of early intermediates in the dioxygen/cytochrome oxidase reaction that had been observed in the initial pump/probe Raman measurements.[7a,b] They noted, however, that photolability maximized at 60–70 μs. Assuming that photolability arose only from the oxy a_3 species, they proposed a kinetic scheme in which rate constants for the reactions in Schemes 4 and 5 above were slower than we have indicated. Our demonstration here that both the oxy and the initial peroxy adducts are photodissociable reconciles the apparent discrepancy, at least qualitatively, as Figure 6 shows that photolability persists well after the oxy species has decayed. Realizing that **4** is also photolabile and using the rate constant we had assigned earlier for its decay, 1×10^4 s^{-1}, provides a good fit with the 10^4 s^{-1} rate constant that Blackmore *et al.*[6h,7e] found in their work for the decay of reaction photolability.

A quantitative discrepancy, however, persists in comparing Figure 6 with the Blackmore *et al.* data, as we predict that photolability maximizes at about 45 μs in the reaction, whereas the optical data show a maximum at somewhat longer times. This discrepancy may be more apparent than real, however, as neither the Cornell group nor we have been able to characterize the photodissociation processes in detail. Light saturation curves for the photoreactions have not been reported, and, thus, whether complete photodissociation was achieved for both **2** and **4** in the two studies is uncertain. Moreover, the apparent photodissociation quantum yields (ϕ) for the two species are unknown. For the oxy complex, we have good precedence for assigning a value of ϕ in the range of a few percent on the basis of O_2 photodissociation yields in other heme O_2 model complexes and proteins[19] (see below). The photolability of the peroxy species **4** is more problematic, as heme–peroxide complexes have not been amenable to detailed study owing to their chemical reactivity.[20] The side-bound peroxy complex that was synthesized and characterized by Valentine and her co-workers[21] is an exception, but its photochemical dynamics have not been characterized. That it may be susceptible to light-driven dioxygen release, however, is suggested by the photochemical activity of a side-bound peroxide/titanium porphyrin system.[22] The photolability of peroxy-bridged cobalt complexes[23] has some analogies with that of the oxidase peroxy species (see below), and by using photodissociation quantum yields observed in these complexes as a guide, values of 1–5% might be expected for **4**. From these arguments, it appears that both the oxy and peroxy species have low photodissociation quantum yields and that achieving complete photodissociation may be difficult. If the peroxy species **4** is somewhat more susceptible to photodissociation than **2**, then subsaturating photolysis pulses will produce yield curves that are shifted toward later times, which may account for the 60–70 μs maximum in the photodissociation yield curve observed by Blackmore *et al.*[6h]

The experimental data and calculated curves for the disappearance of photolability in Figure 6, as well as the optical data on the decay of photolabile species,[6h] indicate that light stable reaction intermediates appear in the 100 μs time range after the reaction has been initiated. Several processes in the enzyme have rate constants that are near 10^4 s^{-1} and, thus, may be responsible for the decay of photolability. These include (a) the protonation reaction detected by the Goteborg group[6i] that we have interpreted to reflect the **4** → **5** process in Figure 1, (b) the equilibration of electrons between the heme *a* and Cu_A sites in the electron input stage of the enzyme, and (c) the relaxation of the enzyme from "output" to "input" proton-pumping configurations, which is required in any proton-translocating protein.[1,4]

At present, it is not possible to decide unequivocally between these alternatives. In particular, transient optical spectra of specific intermediates, which reflect electronic state structure, are not yet at hand, although these are being pursued in several labs. Nonetheless, one piece of important data is available. In the mixed-valence enzyme, the oxygen adduct (equivalent to **2** in Figure 1) is photolabile. Our previous results,[7c] as well as those of Rousseau and co-workers[7f] and of Hill and Greenwood,[6c] show that the lifetime of the mixed valence a_3 oxy species is substantially longer than that of **2** in the fully reduced enzyme and is converted to subsequent intermediates with a rate constant on the order of 6×10^3 s^{-1}. Our earlier results showed that photolability, during the reaction of the mixed-valence enzyme with dioxygen, decays with approximately the same time course. From these observations, we can conclude that the species formed subsequent to the oxy complex in the mixed-valence enzyme, which is generally formulated as a peroxy complex analogous to **3** in Figure 3, is not significantly photolabile. During the studies reported above, we confirmed our earlier observations regarding the disappearance of photolability in the

(17) Mitchell, R.; Rich, P. *Biochim. Biophys. Acta.* In press.
(18) Morgan, J. E.; Verkhovsky, M. I.; Wikström, M. *Biochim. Biophys. Acta* **1994**, *1187*, 106–111.
(19) Welah, A.; Loew, G. *J. Am. Chem. Soc.* **1982**, *104*, 2352–2356.
(20) Balch, A. L. *Inorg. Chim. Acta* **1992**, *198–200*, 297–307.
(21) (a) McCandlish, E.; Miksztal, A. R.; Nappa, M.; Sprenger, A. Q.; Valentine, J. S.; Strong, J. D.; Spiro, T. G. *J. Am. Chem. Soc.* **1980**, *102*, 4268–4269. (b) Burstyn, J. N.; Roe, J. A.; Miksztal, A. R.; Shaevita, B. A.; Lang, G.; Valentine, J. *J. Am. Chem. Soc.* **1988**, *110*, 1382–1384.
(22) Bergamini, P.; Sostero, S.; Traverso, O. *J. Chem. Soc., Dalton Trans.* **1986**, 2311–2314.
(23) Maecke, H. R.; Williams, A. In *Photoinduced Electron Transfer*; Fox, M. A., Chanon, M., Eds.; Elsevier: Amsterdam, 1988; Part D.

mixed-valence enzyme and Hallen *et al.*[24a] have also noted that the "peroxy" species formed by reacting the mixed-valence enzyme with O_2 is stable to illumination.

Thus, in both the fully reduced and mixed-valence enzymes, photolability decays on roughly the same 100 μs time scale, although the dioxygen intermediates are distinct in the two cases. That is, in the reduced enzyme, both the oxy (**2**) and peroxy (**4**) are photolabile, whereas, in the mixed-valence enzyme, only the a_3 oxy complex, analogous to **2**, is photoactive. In the mixed-valence enzyme, the $a^{3+} \rightarrow Cu_A{}^{1+}$ equilibration cannot, of course, occur, which suggests that this is not the dominant factor in controlling photolability. Similarly, Nilsson and co-workers[6i] have shown that formation of the peroxy species in the mixed-valence enzyme is not accompanied by proton uptake from the aqueous phase, which weakens the case for a model in which the **4** → **5** protonation reaction controls light sensitivity. Of the three possibilities discussed above, then, consideration of the mixed-valence data leads to the suggestion that output/input conformational relaxation is the key factor in determining photolability during reaction of the enzyme with O_2. The requirement that the enzyme be in its output configuration for observable photoactivity of the peroxy species **4** most likely arises from the fact that this conformation of the enzyme allows facile and rapid electron transfer between the binuclear center and heme *a*. We argue below that the peroxy species will reform from the photochemically active state, if electron transfer to heme a^{3+} is sluggish.

From the rate of disappearance of photoactivity in the mixed-valence enzyme, we assign a rate for output/input conformational relaxation that is on the order of $6-8 \times 10^3$ s^{-1}. Several other processes have been detected in the enzyme that relax with the same, or a very similar, time constant. These include the following: (a) the first detectable proton uptake from bulk phase during the dioxygen-reduction reaction,[6i] (b) a relaxation phase following CO photodissociation from the mixed valence enzyme that has been assigned as reflecting internal electron transfer within the enzyme,[16,24b,d] and (c) a conformational relaxation that occurs following pulsed laser excitation of the partially reduced enzyme[24c] (both optical absorption and electrical techniques have been used to detect this phase, and its activation parameters are the same as that associated with the protonation reaction in (a) above). Taken together, these observations, along with the photolability data we have presented here, indicate that a functionally significant protein rearrangement occurs on the 80−100 μs time scale following initiation of O_2 reduction by the enzyme. The quantitative assessment of this relaxation time correlates well with the observation that reduction of the peroxy intermediate **3** in the fully reduced enzyme is not coupled to proton translocation (Figure 1). As discussed above and summarized in Scheme 5, the electron-transfer slip occurs with an apparent rate constant of 3×10^4 s^{-1}, which is a factor of 5 faster than the conformational relaxation that is necessary to ensure efficient coupling of the electron transfer to proton translocation.

Electronic and Structural Aspects of Photolability. There is good precedence for photolability in dioxgen/ferrous heme complexes; the phenomenon has been observed and studied extensively in both oxygen-binding heme proteins and heme model compounds. Thus, it is expected that the initial dioxygen adduct in the oxidase/O_2 reaction is photodissociable. It was, in fact, the observation of this photoactivity that led to the first direct experimental support for **2** in the reaction sequence.[7a]

The identity of the photoactive states involved in the light-driven dissociation of O_2 from oxy heme complexes has been addressed computationally,[19] and a reasonably good understanding of the photochemistry has been achieved. The results of these calculations are likely to be relevant to photodissociation in oxidase as well. For oxy heme complexes, two classes of dissociative states have been identified. The first lies higher in energy than the Q-band optical transitions and involves excited states that have $d_\pi \rightarrow d_{z^2}$ or $d_{x^2-y^2} \rightarrow d_{z^2}$ character. The second dissociative class lies lower in energy than the Q-band transitions and involves metal-to-ligand charge-transfer transitions to the lowest unoccupied molecular orbital, which is composed of iron d_{xz} and dioxygen π_v* orbitals. As noted above, the observed quantum yield for O_2 photodissociation is only a few percent in the oxy heme systems. The origin of this behavior remains unclear and both increased excited state relaxation, relative to the carbon monoxide case, and increased geminate recombination have been invoked to account for the low yields. The quantum-chemical calculations also account for the observation in a number of heme proteins and heme models, including cytochrome oxidase, that the ν(Fe−O_2) vibration, but not the O=O stretch of the bound ligand, is enhanced with Soret and Q-band excitation. Direct resonance with the charge-transfer state is necessary to observe the intraligand O=O stretch and, according to the computational results, these states are too low in energy to be in resonance with visible laser excitation.

The photochemical activity that we observe for the peroxy species, **4**, on the other hand, is more surprising and was not expected *a priori*. The photochemical activity of heme peroxy complexes has not been explored extensively. Nakamoto and his co-workers[25] have observed light-induced cleavage of the oxygen−oxygen bond in their low-temperature Raman studies of heme peroxides and Bergamini *et al.*[22] showed that UV irradiation of the side-bound peroxide complex of titanium tetraphenylporphyrin induces elimination of dioxygen. Quantum yields, wavelength dependencies, and the excited states involved in these photochemical activities have not been characterized.

The peroxy complexes of binuclear cobalt(III) complexes have been studied in detail,[23] however, and consideration of the photochemistry of these systems provides insight into the photolability of the cytochrome oxidase peroxy complex. Irradiation throughout the visible region leads to a one-photon process in which both cobalt ions in the complex are reduced, and dioxygen is released by a process that is thought to occur according to Scheme 6,

Scheme 6

$$Co^{III}\text{–}O_2^{2-}\text{–}Co^{III} \xrightarrow{h\nu} Co^{III}\text{–}O_2^{-} + Co^{II} \longrightarrow 2Co^{II} + O_2$$

that is, photoexcitation leads to intracomplex electron transfer to one of the two Co(III) ions and cleavage of one of the Co−O bonds to produce the mononuclear cobalt(III) superoxy complex. This decays thermally to dioxygen and Co(II). Maecke and Williams have summarized spectroscopic and photochemical work on the cobalt peroxy complexes[23] and Tuczek and Solomon[26] have provided additional support for the principal conclusions in a single-crystal, polarized absorption study of monobridged binuclear, cobalt peroxo species. The optical

(24) (a) Hallén, S.; Svensson, M.; Nilsson, T. *FEBS Lett.* **1993**, *318*, 134−138. (b) Oliveberg, M.; Malmström, B. G. *Biochemistry* **1991**, *30*, 7053−7057. (c) Hallén, S.; Brzezinski, P. *Biochim. Biophys. Acta* **1994**, *1184*, 207−218. (d) Hallén, S.; Brzezinski, P.; Malmström, B. G. *Biochemistry* **1994**, *33*, 1467−1472.

(25) (a) Bajdor, K.; Nakamoto, K. *J. Am. Chem. Soc.* **1984**, *106*, 3045−3046. (b) Proniewicz, L. M.; Bruha, A.; Nakamoto, K.; Kyuno, E.; Kincaid, J. *J. Am. Chem. Soc.* **1989**, *111*, 7050−7056.

(26) Tuczek, F.; Solomon, E. I. *Inorg. Chem.* **1992**, *31*, 944−953.

Scheme 7

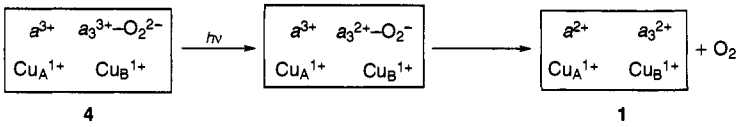

4 1

spectra of these compounds have bands that are assigned as metal-centered d,d transitions and as ligand (peroxy)-to-metal charge-transfer (LMCT) transitions. The latter involve both π_v^* → Co and π_σ^* → Co charge transfers, where π_v^* is the antibonding peroxo orbital that lies out of the plane of the complex and π_σ^* is the corresponding in-plane antibonding orbital. In the monobridged species, only the π_v^* → Co charge-transfer transition, which is assigned as the lowest-energy band in the spectrum, is thought to be effective in initiating the photochemistry in Scheme 6; the photodissociation quantum yield is constant at approximately 3×10^{-2} over the visible wavelength range. Both the intensity and wavelength absorption maximum of the π_v^* → Co charge-transfer transition are sensitive functions of the geometry of the complex. This LMCT transition increases in oscillator strength and shifts to the blue as the complex is distorted from a planar geometry. The picture that emerges, then, from the cobalt peroxy system is that photodissociation proceeds with modest quantum yield from a low-lying charge-transfer state. This CT state can be populated directly or fed by relaxation of higher-lying excited states; its excited-state energy is determined by the geometry of the complex.

A similar scenario can account for the photoactivity we observe for **4** in the cytochrome oxidase/dioxygen reaction. That is, we suggest that there are low-lying ligand-to-metal CT states in the $a_3^{3+}-O_2^{2-}$ species that are populated as the $\pi\pi^*$ excited state, generated by Soret excitation, relaxes. This process is analogous to the light-induced population of the low-lying and photochemically active charge-transfer states in the oxy heme case discussed above. For the peroxy species, however, electron transfer is required for photoproduct formation, and we suggest that these reactions proceed as shown in Scheme 7. Photoexcitation produces the ferrous a_3–superoxide complex $a_3^{2+}-O_2^-$. We presume that this species is strongly reducing and, given that the Cu_B species is already cuprous, relaxes by transferring an electron to the ferric *a* center.[4,61] Subsequent dissociation of O_2, which is bound only loosely in the binuclear center, produces the fully reduced, deoxy enzyme. We expect that the overall yield for the production of the deoxy species will be low, as both relaxation of the $a_3^{2+}-O_2^-$ species to the peroxy and binding of O_2 to produce the oxy complex compete with its formation. The requirement that the enzyme be in its output configuration for observable photolability in **4** is rationalized in the above scheme, as sluggish electron transfer in the second step will not compete effectively against the reversal of the initial photochemical step. Verkhovsky *et al.* have shown that electron transfer between *a* and a_3 can occur with rates $>10^5$ s^{-1} in the output configuration.[16] The $a_3^{2+}-O_2^- \rightarrow a^{3+}$ electron transfer in Scheme 7 is expected to be more strongly driven and, thus, we anticipate a rate of at least this magnitude.

The ν(Fe–his) Vibration in Heme a_3 Photoproducts. The data in Figures 3 and 5 show that photodissociation of carbon monoxy, oxy, and peroxy ligands from a_3 in the binuclear center of the fully reduced enzyme produces the same transient photoproduct. Moreover, recent work by Ondrias, Chan, and co-workers[27] has shown that the transient photoproduct produced by CO photolysis of the mixed valence enzyme strongly resembles that of the fully reduced enzyme. It appears, therefore, that, despite the different electronic states that are involved in the photolysis of the various ligands, the binuclear pocket relaxes to its ground-state configuration along a path that is independent of the identity of the ligand and involves a common intermediate state. In this species, as originally reported by Findsen *et al.*,[15] the Fe–his vibration is Raman active and occurs at 221 cm^{-1}, which is upshifted by 6 cm^{-1} relative to its frequency in the equilibrium reduced, deoxy form of the enzyme; the ν_4 mode of the photoproduct, however, occurs at the same frequency, 1355 cm^{-1}, as that of the relaxed reduced form of the protein. We have not been able to monitor the kinetics by which the transient photoproduct relaxes to equilibrium following oxy and peroxy photodissociation, as this measurement requires a third laser pulse. We anticipate, however, that these relaxation kinetics will occur on the microsecond time scale, as Findsen *et al.*[15] showed for the photoproduct produced by CO photodissociation.

In general, the photoproduct produced by ligand dissociation from heme a_3 has several characteristics that are similar to those of other heme protein photoproducts. These include an upshifted ν(Fe–his) vibration and fairly rapid relaxation kinetics to the ground-state, high-spin, five-coordinate species. Several aspects of the photoproduct in cytochrome oxidase are, however, noteworthy. First, in hemoglobin, there is an inverse correlation between shifts in the frequency of the oxidation state marker mode, ν_4, and that of the Fe–his vibration in the photoproduct, relative to the equilibrium deoxy proteins.[28] In oxidase, as noted above, ν_4 in the photoproduct is unshifted, relative to its frequency in relaxed heme a_3. Second, geminate ligand recombination, which occurs to a considerable extent in the oxygen transport proteins, makes virtually no contribution in oxidase; for heme a_3, ligand rebinding occurs from bulk solution in a second-order process that takes place on the microsecond time scale. Third, in oxidase, Findsen *et al.*[15] have shown that the heme a_3 relaxation process is distinctly biphasic, which suggests a complex mechanism with at least two intermediate species. Fourth, Woodruff and co-workers[11] have studied the CO photodissociation process in the fully reduced oxidase and have shown that the intensity of the Fe–his mode in the photoproduct is a function of laser probe intensity. From this, they suggested that a ligand shuttle mechanism occurs that involves distal/proximal ligand exchange at the a_3 center following CO photolysis. These differences provide insight into unique aspects of cytochrome oxidase structure and function.

The correlation that occurs between ν_4 and ν(Fe–his) in hemoglobin CO photolysis products was initially interpreted in terms of the geometry of the proximal histidine and, particularly, its tilt angle θ with respect to the heme plane.[28,29] As θ deviates from 90°, mixing of $\sigma(Fe-N_{his})$ and $e_g(\pi^*)$ molecular orbitals occurs; this mixing was proposed to affect both the coupling of the out-of-plane Fe–his stretching vibration and the frequen-

(27) Lou, B.-S.; Larsen, R. W.; Chan, S. I.; Ondrias, M. R. *J. Am. Chem. Soc.* **1993**, *115*, 403–407.

(28) Rousseau, D. L.; Friedman, J. M. In *Biological Applications of Raman Spectroscopy*; Spiro, T. G., Ed.; John Wiley and Sons, Inc.: New York, 1988; Vol. 3, pp 294–346.

(29) (a) Bangcharoenpaurpong, O.; Schomaker, K. T.; Champion, P. M. *J. Am. Chem. Soc.* **1984**, *106*, 5688–5698. (b) Champion, P. M. In *Biological Applications of Raman Spectroscopy*; Spiro, T. G., Ed.; John Wiley and Sons, Inc.: New York, 1988; Vol. 3, pp 249–292. (c) Friedman, J. M.; Campbell, B. F.; Noble, R. W. *Biophys. Chem.* **1990**, *37*, 43–59.

cies of ν_4 and ν(Fe−his). Thus, relaxation in the photoproduct was correlated with relaxation in the tilt angle of the proximal histidine in the oxygen transport proteins. Stavrov[30] re-examined the photoproduct situation recently and extended these earlier ideas substantially. He concludes that both the tilt angle, θ, and the out-of-plane displacement of the Fe, q, are critical coordinates in the dynamics of heme protein relaxation. He concludes that changes in θ introduce $\sigma(\text{Fe}-\text{N}_{\text{his}})-\text{e}_g(\pi^*)$ mixing, which populates the $\text{e}_g(\pi^*)$ antibonding orbital and affects the ν_4 frequency. Out-of-plane displacement, q, on the other hand, mixes both $\text{a}_{1g}(\text{d}_{z^2}/\text{a}_{2u}(\pi)$ and $\sigma(\text{Fe}-\text{N}_{\text{his}})/\text{a}_{2u}(\pi)$ and affects primarily the frequency and resonance enhancement of the ν(Fe−his) mode. Moreover, he also notes that both proximal ligand hydrogen bonding effects and steric interactions will complicate the dynamic behavior that occurs during heme pocket relaxation. If relaxations along q and θ are coupled, then a correlation between ν_4 and ν(Fe−his) is expected. This appears to be the situation in the oxygen transport proteins. If, however, changes along the tilt coordinate are small, then relaxation along the out-of-plane coordinate dominates and no *a priori* correlation between ν_4 and ν(Fe−his) is predicted. This appears to be the case for heme a_3 relaxation, which suggests that, as opposed to hemoglobin, in cytochrome oxidase, ligand binding and dissociation are not accompanied by significant changes in the angular orientation of the histidine ligand.

The discussion above focused on the transient intermediate that is detected when CO, oxy, or peroxy heme a_3 is photolyzed and interrogated with high-power probe pulses. When low-power photolysis and probe pulses are used, however, the heme a_3−CO complex exhibits complex photodynamics. Woodruff and co-workers[11,12] performed a series of spectroscopic studies on the photodissociation process and noted reduced ν(Fe−his) resonance enhancement under low-power conditions. From this work, they concluded (1) transient binding of CO to Cu_B and (2) binding (<1 ns) of a photolabile endogenous ligand, which was displaced from Cu_B subsequent to CO binding, to cytochrome a_3. The behavior of the mixed-valence CO, however, contrasts with that observed for fully reduced CO. In the mixed-valence species, the intensity of the Fe−his mode in the photoproduct, measured against the intensity of ν_4 or ν_8, is not a function of the laser-probe intensity.[27] Whether the behavior of the CO photoproduct, as a function of laser probe power and protein redox state, reflects ligand exchange processes or is a manifestation of the complex dependence of ν(Fe−his) mode intensity on the details of the coordination geometry of the axial histidine, as discussed above, remains an open question to be addressed in future work.

It now appears that the oxidase/oxygen reaction can be broken down into at least two distinct series of events: (1) oxygen binding and trapping and (2) imposition of proton control on the coupled electron and proton transfers that produce proton translocation. The results here, as well as corresponding optical data, indicate that we now have a reasonable understanding of the first process. This situation provides an excellent foundation from which to dissect the underlying mechanisms for the second, and more interesting, set of reactions.

Acknowledgment. This work was supported by NIH Grant No. GM25480. We are grateful to Yong Zhang for preliminary measurements and to Professor Q. Gibson for a helpful discussion. The experimental work was performed at Michigan State University.

Note Added in Proof: While this manuscript was in review, two groups (Iwata, S.; Ostermeier, C.; Ludwig, B.; Michel, H. *Nature* **1995**, *376*, 660−669. Tsukihara, T.; Aoyama, H.; Yamashita, E.; Tomizaki, T.; Yamaguchi, H.; Shinzawa-Itoh, K.; Nakashima, R.; Yaono, R.; Yoshikawa, S. *Science* **1995**, *269*, 1069−1074) reported high-resolution crystal structures of cytochrome oxidase. The close approach of the heme *a* and heme a_3 macrocycles that is apparent in both structures provides a basis for the rapid $a \leftrightarrow a_3$ electron transfer determined in the data reported here.

JA943306C

(30) Stavrov, S. *New J. Chem.* **1993**, *17*, 71−76.